K-shell spectra from Ag, Sn, Sm, Ta, and Au generated by intense femtosecond laser pulses

ARTICLE *in* HIGH ENERGY DENSITY PHYSICS · MAY 2007

Impact Factor: 1.23 · DOI: 10.1016/j.hedp.2007.02.022

9 AUTHORS, INCLUDING:

J. F. Seely
Artep Inc and Space Systems Research Cor…
420 PUBLICATIONS **5,172** CITATIONS
SEE PROFILE

Csilla I. Szabo
National Institute of Standards and Techno…
69 PUBLICATIONS **317** CITATIONS
SEE PROFILE

Hye-Sook Park
Lawrence Livermore National Laboratory
392 PUBLICATIONS **5,656** CITATIONS
SEE PROFILE

Available online at www.sciencedirect.com
ScienceDirect
High Energy Density Physics 3 (2007) 263–271
High Energy Density Physics
www.elsevier.com/locate/hedp

K-shell spectra from Ag, Sn, Sm, Ta, and Au generated by intense femtosecond laser pulses

John F. Seely [a,*], Glenn E. Holland [b], Lawrence T. Hudson [c], Csilla I. Szabo [c,d], Albert Henins [c], Hye-Sook Park [e], Prav K. Patel [e], Riccardo Tommasini [e], J. Martin Laming [a]

[a] *Naval Research Laboratory, Space Science Division, Washington DC 20375, USA*
[b] *SFA Inc., 2200 Defense Highway, Suite 405, Crofton, MD 21114, USA*
[c] *National Institute of Standards and Technology, Gaithersburg, MD 20899, USA*
[d] *Laboratoire Kastler-Brossel, Ecole Normale Supérieure et Université Pierre et Marie Curie, Case 74, 4 Place Jussieu, 75252 Paris Cedex 05, France*
[e] *Lawrence Livermore National Laboratory, Livermore, CA 94551, USA*

Available online 7 February 2007

Abstract

K-shell X-ray spectra were recorded by the Dual Crystal Spectrometer (DCS) from Ag, Sn, Sm, Ta, and Au planar foil targets irradiated by single intense femtosecond pulses from the Titan laser at Lawrence Livermore National Laboratory. DCS implements two quartz crystals in transmission (Laué) geometry covering the X-ray energy range 10–50 keV and 20–120 keV. The spectral images were recorded on photo-stimulable phosphor image plates and on film/phosphor cassettes. The Kα and Kβ spectral lines of Ag with energies 22 keV and 25 keV, Sn at 25 keV and 28 keV, Sm at 40 keV and 46 keV, Ta at 57 keV and 66 keV, and Au at 67 keV and 79 keV were clearly resolved. The observation of these spectral lines, resulting from 1s electron vacancies created by electrons with energies up to at least 80 keV, enables the implementation of K-shell spectroscopy diagnostic techniques for understanding the laser energy deposition, energetic electron generation, ionization distribution, and X-ray conversion efficiency in plasmas produced by an intense femtosecond laser pulse. Based on the measured energies of the Au K-shell transitions, we conclude that the observed Au K-shell transitions are from ionization stages lower than Au^{+44}, and are most likely from neutral Au atoms, that the Titan plasmas and the hard X-ray emissions are dominated by electrons with energies exceeding 80 keV, and that thermal processes play a minor role.

PACS: 52.50.Jm; 52.59.Px; 52.70.La; 07.85.Nc

Keywords: X-ray spectroscopy; Laser–plasma interaction; Hard X-rays; Femtosecond laser

1. Introduction

Transmission crystal (Laué) X-ray spectrometers have been developed to record the hard X-ray spectra generated by irradiating targets with intense laser pulses. The High Energy X-Ray Spectrometer (HXS) implemented a cylindrically bent quartz (10–11) crystal covering the 12–60 keV energy range with moderate ($E/\Delta E \approx 100$) resolving power [1,2]. The High Energy Electronic X-Ray (HENEX) Spectrometer implemented a curved quartz (10–11) crystal covering the 11–40 keV range with >300 resolving power along with four reflection crystals covering lower energy ranges [3–5]. These instruments were based on spectrometers developed at the National Institute of Standards and Technology (NIST) for the measurement of the peak kilovoltage of medical X-ray sources [6–8].

Described in this paper are the initial spectra recorded by a new spectrometer named Dual Crystal Spectrometer (DCS)

* Corresponding author. Tel.: +1 202 767 3529; fax: +1 202 404 7997.
E-mail address: john.seely@nrl.navy.mil (J.F. Seely).

1574-1818/$ - see front matter © 2007 Elsevier B.V. All rights reserved.
doi:10.1016/j.hedp.2007.02.022

that implements two curved transmission crystals covering the 10–50 keV and the 20–120 keV energy ranges. K-shell spectra were recorded from metal foil targets, irradiated by single pulses from the Titan femtosecond (fs) laser at Lawrence Livermore National Laboratory (LLNL), having atomic numbers in the range 47–79: Ag, Sn, Sm, Ta, and Au. The observation of these spectral lines, resulting from 1s electron vacancies created by electrons with energies up to at least 80 keV, enables the implementation of K-shell spectroscopy diagnostic techniques for understanding the laser energy deposition, energetic electron generation, ionization distribution, and X-ray conversion efficiency in plasmas produced by an intense femtosecond laser pulse. Practical applications of this work are hard X-ray radiography of dense targets related to inertially confined fusion and propagation of energetic electron beams for fast ignition [9].

Measurements of the hard X-ray emissions from laser-produced plasmas are often performed using non-dispersive X-ray detectors with filters that establish X-ray energy bandpasses or using a solid-state detector (e.g., CCD) in the single photon per pixel mode. In general, the use of a dispersive X-ray spectrometer, producing a high resolution X-ray spectrum of the line and continuum radiation, is superior to using a non-dispersive detector that produces low resolution data that are subject to modeling and interpretation.

Priedhorsky et al. [10] utilized a low resolution Laué crystal spectrometer to record the K-shell spectra from Au targets irradiated by the HELIOS 10.6 μm laser. The spectrometer consisted of a flat LiF crystal covering the 60–300 keV energy range with resolving power $E/\Delta E \approx 10$. The targets were 300 μm diameter Au microballoons and were irradiated by 6.5 kJ laser pulses with 0.75 ns duration and focused to 10^{16} W/cm^2 intensity. The Au Kα and Kβ spectral lines at 67 keV and 79 keV, respectively, were recorded.

Hölzer et al. [11] recorded Ta K-shell spectra using flat and cylindrically bent Si crystals in the Bragg (reflection) and Laué (transmission) geometries. The Ta targets were irradiated by a Ti:sapphire laser (790 nm wavelength) which produced 150 mJ per pulse and 150 fs pulse duration. The number of laser shots required to produce a well-exposed spectrum was in the range 6000–9000.

Andersson et al. [12] utilized a curved silicon crystal in Laué geometry to record the Sn and Ta K-shell spectra from targets irradiated by a fs duration Ti:sapphire laser focused to an intensity of 5×10^{17} W/cm^2. Typically 300 laser shots were required to produce a well-exposed spectrum. Toth et al. [13] also utilized a Ti:sapphire laser (600 mJ pulse energy, 60 fs pulse duration) and presented multi-shot spectra of Mo and Ta recorded by a NIST Laué spectrometer.

Shown in Fig. 1 is a schematic of the transmission crystal modules utilized in the HXS, HENEX, and DCS spectrometers. X-rays are incident on a cylindrically bent crystal, are diffracted through a slit, and are recorded by a planar detector near the Rowland circle. Metal filters placed at the slit provide K absorption edges in continuum spectra for in situ calibration of the X-ray energy scale. A pinhole with separate filtration is on the center axis of the spectrometer and produces an image

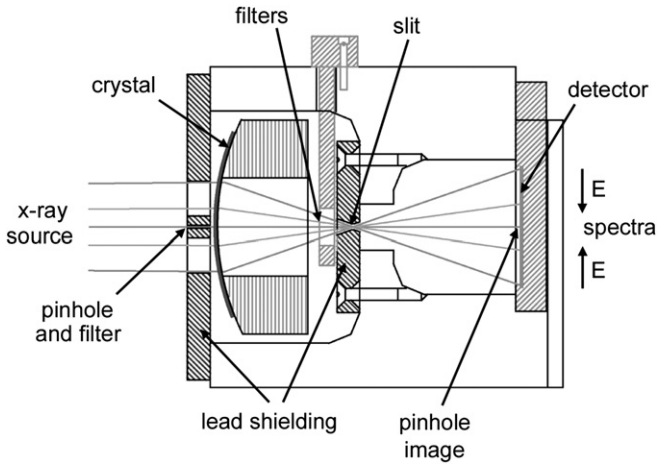

Fig. 1. Schematic of the transmission crystal spectrometer module.

of the source. The relative positions of the pinhole image and the dispersed spectral image indicate the instrument pointing. Massive lead shielding is present on the front of the module and at the slit, and there is no line-of-sight path (except through the pinhole) between the source and detector. This geometry facilitates shielding of the detector from the energetic X-rays, protons, and electrons produced by intense fs laser pulses.

As shown in Fig. 2, DCS implements two quartz (10–11) crystals. The channel 1 crystal is bent to a radius of 119 mm and covers 10–50 keV, and the channel 2 crystal has radius 254 mm and covers 20–120 keV. An alignment laser propagates through pinholes at the rear and front of the instrument and is used to position the spectrometer axis on the target position.

2. Test spectra

The DCS spectrometer was extensively tested at NIST using a W anode X-ray source prior to recording spectra at the Titan laser. Spectral images were recorded on several media: Fuji BAS-SR BaF(Br,I):Eu^{2+} photo-stimulable phosphor image plates, Kodak Biomax film, and medical X-ray film and phosphor screen combinations. Shown in Fig. 3 are spectral images recorded by the DCS channels 1 and 2 on image plates (IPs) using 250 kV peak voltage, 4 mA current, and 40 s

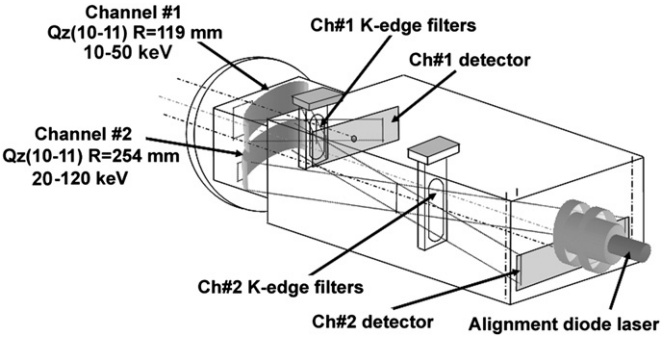

Fig. 2. Design of the two-channel DCS spectrometer.

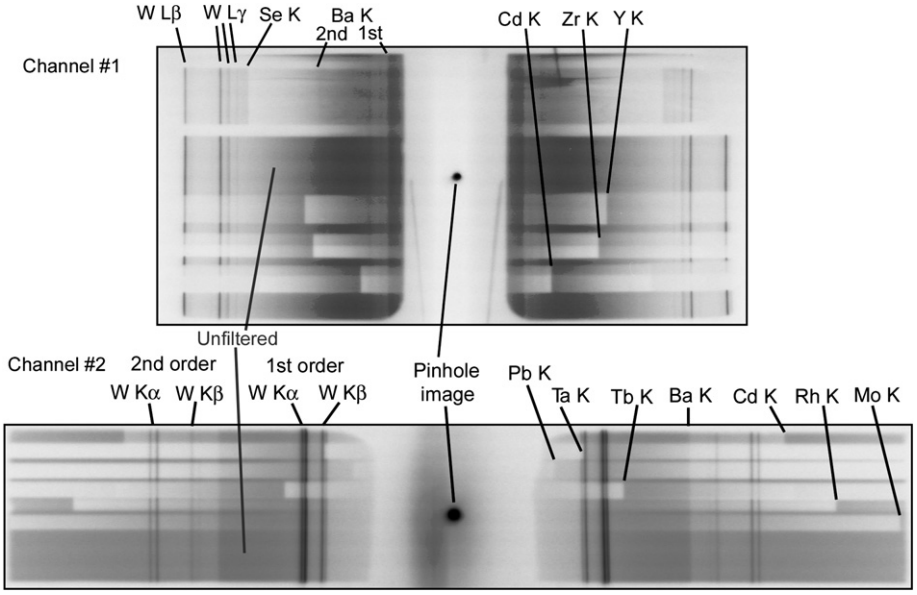

Fig. 3. DCS channel 1 (top) and channel 2 (bottom) X-ray spectral images from a W anode laboratory source showing the characteristic neutral-atom X-ray transitions, filter K absorption edges, and the Ba K edge from the image plates.

exposure time. The DCS crystals were 1.2 m from the W anode, the same distance used subsequently in the Titan laser experiments. Visible on each spectral image shown in Fig. 3 are the pinhole image and two spectra that are symmetric on the left and right sides of the pinhole image. The X-ray energy increases from the two ends of the spectra toward the pinhole image. Channels 1 and 2 cover the W L-shell and K-shell transitions, respectively.

Indicated in Fig. 3 are the K absorption edges produced by filters covering portions of the DCS channel 1 and channel 2 slits. The tabulated K edge energies are listed in Table 1 for the filters Se, Y, Zr, Mo, Rh, Cd, Tb, Ta, and Pb [14]. Also visible is the K absorption edge of Ba, a constituent of the IP. The exposure on the high energy side of the Ba K edge is enhanced by increased absorption in the IP at these energies, [15] while the exposures on the high energy sides of the filter K edges are diminished because of increased absorption by the filters positioned at the spectrometer slits.

In the channel 1 spectral image shown in Fig. 3, faint diagonal features appear below and on both sides of the pinhole, and exposure appears on the left side of the pinhole image in the channel 2 spectral image. These features were caused by off-axis X-rays propagating through the DCS entrance apertures and the wide slits used during the instrument test phase, and possibly by slight misalignments of the slits. These artifacts were reduced by adjusting the slits prior to the Titan laser experiments and by implementing a collimation tube between the laser-irradiated targets and the spectrometer.

Table 1
The K absorption edge energies observed in Fig. 3 in keV (Ref. [14])

Se	12.655
Y	17.037
Zr	17.996
Mo	20.000
Rh	23.222
Cd	26.713
Ba	37.452
Tb	52.004
Ta	67.404
Pb	88.006

Based on the geometry of the bent crystal that has left–right symmetry about the spectrometer axis (and the pinhole image), the energy scale can be approximated by the function (derived in Ref. [8])

$$E^2 = a + b/(x - x_o)^2 + c(x - x_o)^2 \quad (1)$$

where $x - x_o$ is the lateral distance from the center (x_o) of the spectral image. The parameters a, b, c, and x_o were determined by simultaneously fitting the W transition energies and the K edge energies in the left and right spectra using the least squares technique. The W K-shell and L-shell transition energies and the K edge energies were from Ref. [14].

Shown in Fig. 4(a) is the column summation of the channel 1 spectral image of Fig. 3, where the summation is over the unfiltered portion of the spectral image at and just above the pinhole image. The W Lβ and Lδ transitions and the 1st and 2nd order Ba K edges are indicated. Shown in Fig. 4(b) are the spectra summed over the Y filter region on the left and right sides of the pinhole image as functions of energy. The detailed W Lβ and Lδ spectra from Fig. 4(b) are shown in Fig. 4(c). The standard deviation of the differences between the fitted energy scale and the tabulated W transition and K edge energies is 30 eV, and this represents the accuracy of the channel 1 energy scale.

Shown in Fig. 5(a) is the column summation of the channel 2 spectral image of Fig. 3, where the summation is over the unfiltered portion of the spectral image below the pinhole

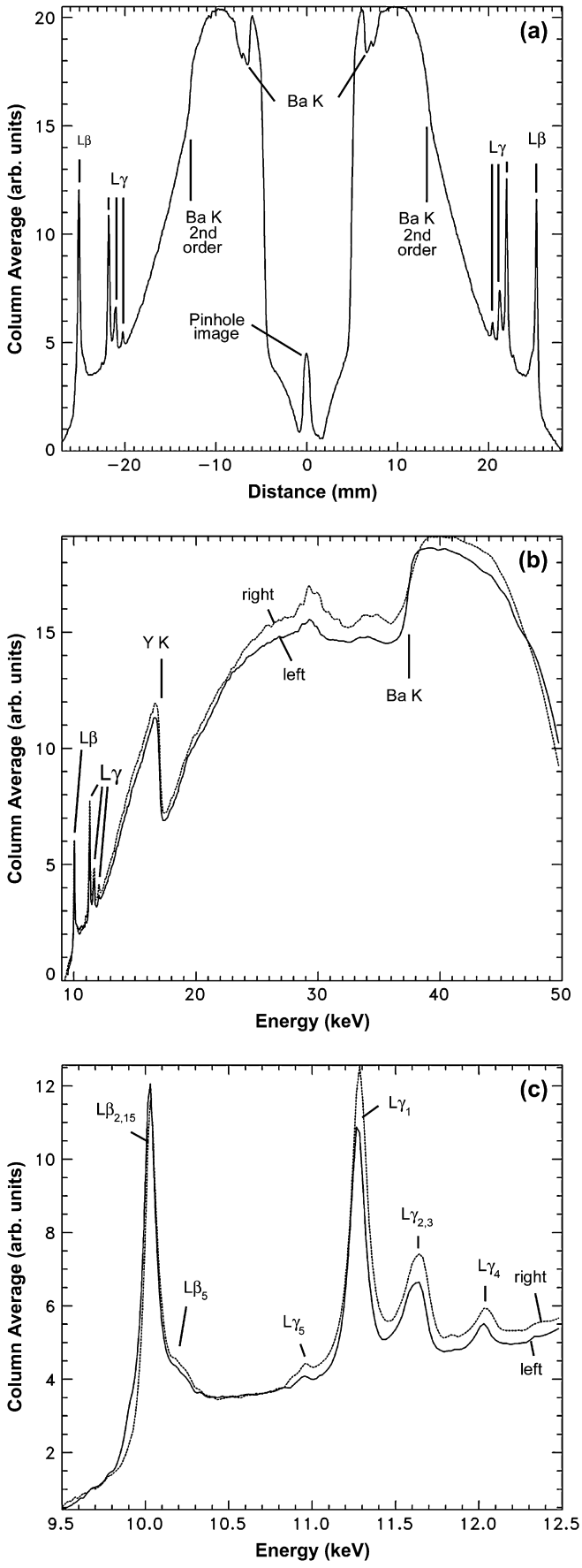

Fig. 4. (a) DCS channel 1 W spectrum as a function of distance from the pinhole image, (b) W spectra on the left and right sides of the pinhole image as functions of energy, and (c) identification of the W L-shell transitions.

image. The 1st and 2nd order W Kα and Kβ transitions and the 1st order Ba K edge are indicated. Shown in Fig. 5(b) are the left and right side spectra as functions of X-ray energy. The 2nd order W spectra from Fig. 5(b) are shown in Fig. 5(c), where the (1st order) energy scale is that derived from the filter K edges and the Ba K edge. Resolved in Fig. 5(c) are the W $K\alpha_1$, $K\alpha_2$, $K\beta_1$, and $K\beta_2$ lines with transition energies listed in Table 2. The standard deviation of the differences between the fitted energy scale and the tabulated W transition energies and the K edge energies is 60 eV, and this represents the accuracy of the channel 2 energy scale.

The left side spectra in the channel 2 spectra (Fig. 5) are slightly brighter than the right side spectra, while the channel 1 right side spectra are brighter (Fig. 4). These brightness differences could be caused by small differences in the alignment of the channels 1 and 2 crystals and slits to the instrument axis and a small error in the pointing of the instrument axis to the W anode. This could be corrected by more testing and tuning of the spectrometer components.

3. Laser-produced spectra

K-shell spectra from metal foil targets with atomic number in the 47 (Ag) to 79 (Au) range were recorded at the LLNL Titan laser facility[16]. The Titan laser produced up to 300 J per pulse, and approximately 50% of the laser energy was focused by a near normal incidence parabolic mirror into a 10 μm spot.

A variety of targets were irradiated with laser pulse durations ranging from 0.5 ps to 120 ps. The targets consisted of metals foils of 0.1–4 mm size and 5–50 μm thickness, and some targets had thin coatings of lower-Z materials and grids mounted near the foil surface. The brightest K-shell spectra were produced by using the shorter pulse durations, providing up to 10^{21} W/cm^2 intensity at the center of the focal spot, and using the larger, thicker target foils.

DCS was positioned outside the Titan target chamber and viewed the target through a port with a Lexan vacuum window. For the spectra shown here, DCS viewed the target's irradiated (front) side with a source-to-crystal distance of 1.2 m and an angle of approximately 30° from the normal to the target surface. Spectra were initially recorded by viewing the back side of the target, but these spectra had lower line to continuum ratios compared to the spectra recorded when viewing the front side of the target.

The targets irradiated by Titan laser pulses were intense sources of hard X-rays and energetic particles that fluoresced metal objects in the target chamber. As a result, it was necessary to implement a collimation tube inside the Titan target chamber to limit the DCS field of view for the purpose of attenuating fluorescence from nearby objects. An aperture, consisting of lead and Lexan, was mounted on the front end

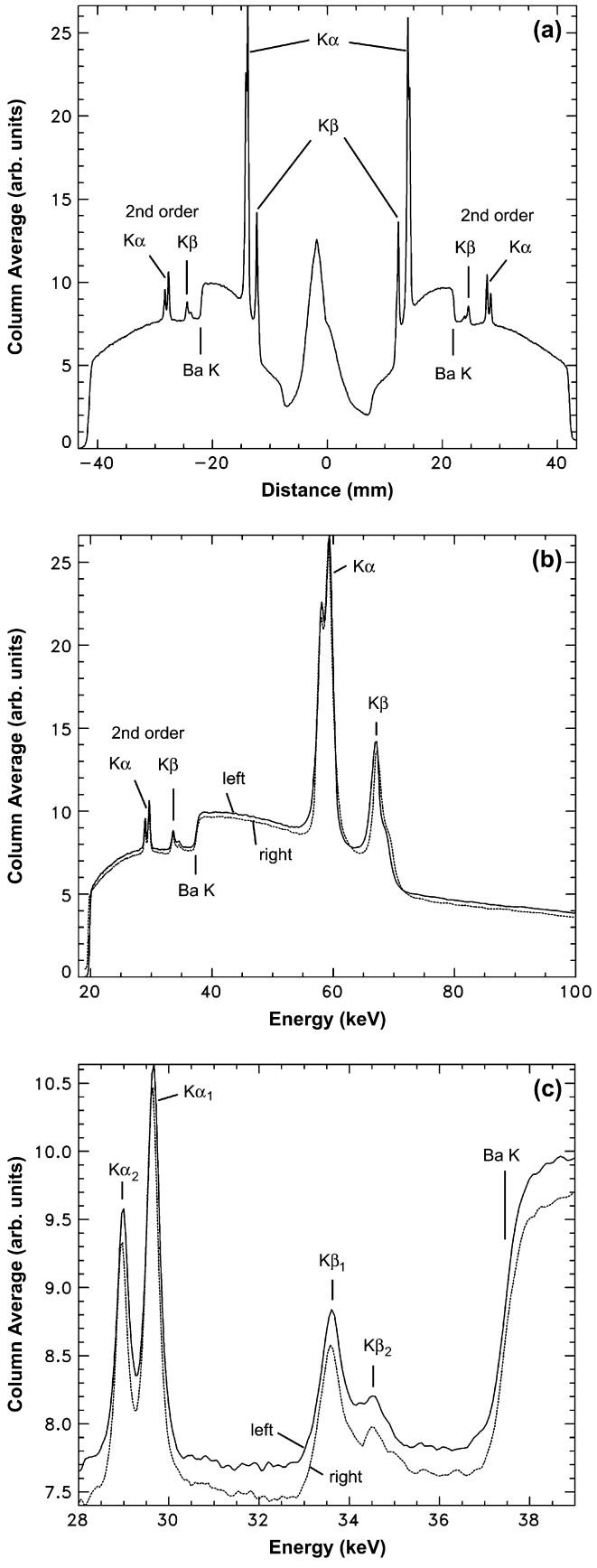

Fig. 5. (a) DCS channel 2 W spectrum as a function of distance from the pinhole image, (b) W spectra on the left and right sides of the pinhole image as functions of energy, and (c) 2nd order W spectra with the (1st order) energy scale determined from the K absorption edges.

of the collimation tube and 30 cm from the target. This collimation tube greatly reduced the background hard X-ray exposure in the spectra as well as asymmetric exposure near the channel 2 pinhole image that resulted from off-axis rays from objects in the Titan chamber and passing undiffracted through the channel 2 slit (as seen in the Fig. 3 NIST test image taken before implementation of the collimation tube).

Spectra recorded on image plates by the DCS channel 1 crystal from Ag and Sm foil targets are shown in Fig. 6, where the intensities are in arbitrary units and are normalized to 100 at peak intensity. The 1st and 2nd order Kα and Kβ transitions are clearly resolved in the Ag spectrum. The Sm spectrum is fainter than the Ag spectrum, the 2nd order Sm Kα feature is very weak, and the 2nd order Kβ feature is not detected.

The energy scales in Fig. 6 were calculated using Eq. (1) and the parameters a, b, and c that were derived from the W spectra recorded by the channel 1 crystal during NIST testing as shown in Fig. 4(b). The centers (x_o) of the Ag and Sm spectra were assumed to be the midpoint of the Kα and Kβ features in the left and right side spectra. Using these energy scales, the measured energies of the Ag and Sm Kα and Kβ features are in good agreement with the neutral-atom tabulated values listed in Table 2. This implies that the Ag and Sm Kα and Kβ features are most likely transitions in neutral atoms. It is possible that the Ag and Sm Kα and Kβ features are, or include, transitions in low charge states sufficiently close to neutral so that the energy shifts from the neutral-atom transitions are within the energy resolution of the instrument.

An Au spectral image recorded at the Titan laser is compared to the W spectral image recorded during instrument testing at NIST in Fig. 7, where both images were recorded by channel 2 and on image plates, and the source-to-crystal distance was 1.2 m. While the 1st order Au Kα and Kβ lines are present in the Titan spectrum, this spectrum is fainter than the NIST spectrum, and the 2nd order Au lines are not present in the Titan spectrum. Other spectra (not shown here) were recorded by the DCS channel 2 crystal from Sn and Ta targets irradiated by Titan laser pulses.

The left and right side 1st order Au and W spectra are compared in Fig. 8(a) and (b). The Au energy scale was calculated using Eq. (1) and the parameters a, b, and c that were derived from the W spectrum. The center (x_o) of the Au spectrum was assumed to be the midpoint of the Au Kα and Kβ features in the left and right side spectra. The energies of the Au Kα and Kβ features are in good agreement with the neutral-atom tabulated values listed in Table 2. As for the DCS channel 1 Ag and Sm spectra, this implies that the Au Kα and Kβ features are most likely transitions in neutral Au atoms, but it is possible that the Au Kα and Kβ features are, or include, transitions in low charge states sufficiently close to neutral so that the transition energies are within the energy resolution of the instrument.

Table 2
The neutral-atom transition energies and binding energies in keV (Ref. [14])

Transition			Ag	Sn	Sm	Ta	W	Au	U
$K\alpha_2$	$K\text{-}L_2$	$1s_{1/2}-2p_{1/2}$	21.990	25.044	39.523	56.278	57.982	66.991	94.651
$K\alpha_1$	$K\text{-}L_3$	$1s_{1/2}-2p_{3/2}$	22.163	25.271	40.118	57.533	59.319	68.805	98.432
$K\beta_1$	$K-M_3$	$1s_{1/2}-3p_{3/2}$	24.942	28.486	45.413	65.223	67.245	77.980	111.295
$K\beta_2$	$K-N_3$	$1s_{1/2}-4p_{3/2}$	25.457	29.110	46.575	67.014	69.101	80.186	114.607
Binding energy		$1s_{1/2}$	25.516	29.200	46.849	67.404	69.509	80.721	115.601

As seen in Fig. 8(a), the Au $K\alpha_1$ and $K\alpha_2$ features, near 67 keV and with 1814 eV separation as listed in Table 2, are resolved, while the Au $K\beta_1$ and $K\beta_2$ features near 79 keV and with 2206 eV separation are not resolved. In Fig. 8(b), the W $K\alpha_1$ and $K\alpha_2$ features near 59 keV and with 1337 eV separation are resolved, and the line widths are 600 eV. The W $K\beta_1$ and $K\beta_2$ features near 68 keV and with 1856 eV separation are just resolved. The lower resolution of the observed Au Kβ transitions, compared to the Kα transitions with smaller energy separation, may result from the lower Kβ intensities and from possible blending with additional (weaker) Kβ transitions such as the $K-M_2$ ($1s_{1/2}-3p_{1/2}$) and $K-N_2$ ($1s_{1/2}-4p_{1/2}$) transitions. In any case, the 600 eV Kα line widths indicate that the DCS resolving power is approximately 100 in the 1st diffraction order in this energy region.

The 2nd order W spectrum is plotted in Fig. 8(c), with an energy scale corresponding to the 1st order energy, and may be compared to the 1st order Au and W spectra shown in Fig. 8(a) and (b), respectively. The W $K\alpha_1$ and $K\alpha_2$ transitions (1337 eV separation) and the $K\beta_1$ and $K\beta_2$ transitions (1856 eV separation) are well resolved in the 2nd order spectrum, and the line widths are 400 eV (using the 1st order energy scale). Thus the DCS channel 2 resolving power is approximately 150 in the 2nd diffraction order in this energy region.

In Fig. 8(a), the Au left spectrum is significantly brighter than the right side spectrum, while the W spectra in Fig. 8(b) are approximately equal. This implies the brightness of the Au left spectrum is real exposure and is not an artifact. In addition, the Au left side spectrum has a broad exposure centered on the Au Kα feature, which is absent in the Au right spectrum and in the W spectrum. A similar broad exposure appears symmetric around the Au pinhole image in Fig. 7. These

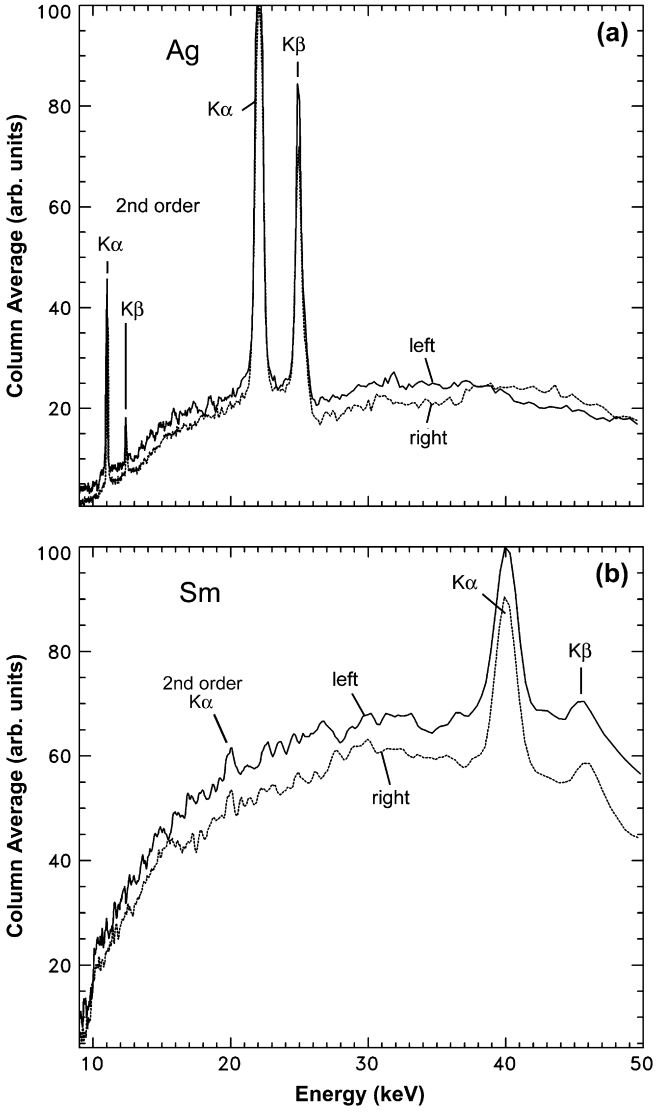

Fig. 6. Spectra from (a) Ag and (b) Sm targets irradiated by single Titan laser pulses and recorded by the DCS channel 1, where the intensities are in arbitrary units and are normalized to 100 at peak intensity.

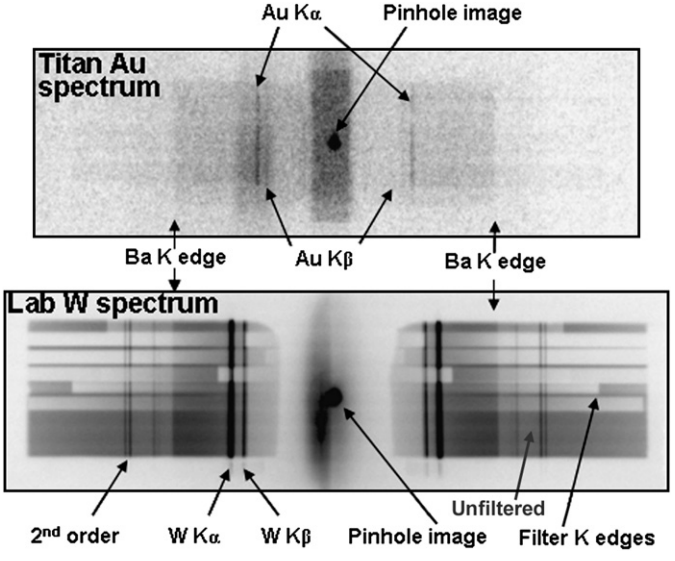

Fig. 7. Comparison of the Au spectral image recorded with Titan laser irradiation and the W spectral image recorded using an NIST X-ray source, both recorded by DCS channel 2.

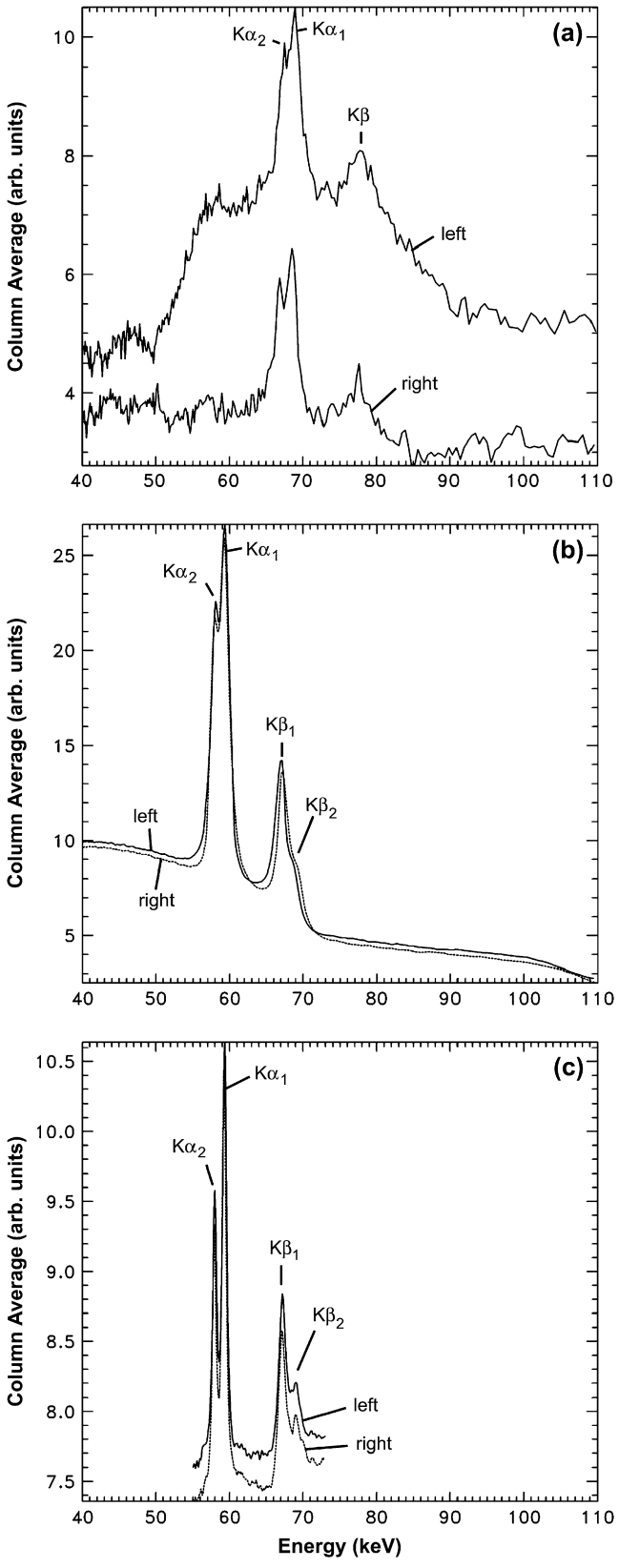

Fig. 8. (a) Au spectrum recorded using Titan laser irradiation, (b) 1st order W spectrum recorded using a NST X-ray source, and (c) 2nd order W spectrum. All spectra were recorded by DCS channel 2.

two broad exposure features in the spectra from Titan-irradiated Au targets are believed to be images of the DCS channel 2 slit produced by X-rays with sufficient energy (>500 keV) to penetrate the DCS front-end shielding (thickness 9.5 mm) that surrounds the DCS pinhole (see Fig. 1). The broad exposure feature symmetric about the pinhole image in Fig. 7 (top image) is caused by hard X-rays from the Titan target, and the broad exposure feature in the left side spectrum is from a fluorescing object to the right of the Titan target as viewed by DCS. These broad features could be reduced by using additional lead shielding, reducing the width of the channel 2 slit, and reducing the field of view of the collimation tube.

4. Discussion

Kα and Kβ spectra from metal foil targets with atomic numbers in the range 47 (Ag) to 79 (Au) were recorded using single shots of the Titan laser with typically 300 J energy and 10^{21} W/cm^2 intensity at the center of the focal spot. This is the first systematic study of K-shell spectroscopy covering a broad range of heavy metal targets irradiated by single fs laser pulses and using a dispersive spectrometer with relatively high resolving power (150).

It was necessary to shield the spectrometer with massive lead sheets and to implement a collimation tube that attenuated the hard X-ray fluorescence from objects near the target. The time-integrated X-ray dose was measured by pocket dosimeters sensitive to X-rays with energy >15 keV. The single-shot dose measured in front of the spectrometer crystals (and outside the Lexan vacuum window) was typically 140 mR, and the dose measured at positions beside the spectrometer and through the target chamber wall averaged 15 mR. This X-ray dose, as well as the broad exposure features observed in the DCS channel 2 spectral images resulting from penetration of the lead shielding, indicate continuum X-ray energies >500 keV.

As listed in Table 2, the observed Kα and Kβ spectral features are transitions of the type 1s–2p, 1s–3p, and 1s–4p. The measured transition energies indicate that the observed transitions are in neutral atoms, or possibly in ions with low ionization and with energy shifts from the neutral-atom transitions that are too small to be resolved in this study.

In order to estimate the ability of DCS to distinguish transitions in Au ionization stages, transition energies were calculated using the HULLAC atomic physics code [17]. Owing to the complexity of the calculation, only ions with outer ns^2np^6 closed shells and a 1s vacancy were considered, where $n = 2$, 3, 4, and 5: Au^{+70}, Au^{+62}, Au^{+44}, and Au^{+26}. Listed in Table 3 are the ground configurations, the calculated transition energies, and the energy shifts from the Au neutral-atom transitions. It was found that the 1s–2p type transitions in Au^{+26} were indistinguishable from the neutral-atom energies, and the Au^{+26} transitions are not listed in Table 3.

While the HULLAC transition energies may differ from the experimental transition energies, the calculated differences in energy with ionization stage are expected to have high accuracy, and this is the quantity of interest for estimating the

Table 3
The transition energies calculated using the HULLAC atomic physics code, and the energy shifts from the Au neutral-atom transition energies (in eV)

Ion	Ground configuration	Transition			
		$1s_{1/2}-2p_{1/2}$	$1s_{1/2}-2p_{3/2}$	$1s_{1/2}-3p_{3/2}$	$1s_{1/2}-4p_{3/2}$
Au^{+44}	$[Au^{+62}]3d^{10}4s^24p^6$	67086 (+95)	68924 (+119)	78735 (+755)	81763 (+1577)
Au^{+62}	$[Au^{+70}]3s^23p^6$	67112 (+121)	68954 (+149)	78775 (+795)	
Au^{+70}	$1s2s^22p^6$	67351 (+360)	69226 (+421)		

ability of DCS to resolve transition energy shift with ionization. As seen in Table 3, the energy shift of 1s–2p Kα transitions in Au^{+44} from the neutral-atom transitions is approximately 100 eV. The energy shifts of the Au^{+44} 1s–3p and 1s–4p transitions are 755 eV and 1577 eV, respectively. Considering the 60 eV accuracy of the DCS channel 2 1st order energy scale and the 600 eV instrumental width, the Au^{+44} energy shifts could be observed by DCS. Since the Kα and Kβ transition energies in the Au spectra were consistent with the neutral-atom transition energies, we conclude that the observed transitions originated in Au ions with lower charge than Au^{+44}.

The observed transitions are believed to result from 1s vacancies created by energetic electron impact. Thus the Au^{+44} transitions listed in Table 3 result from the removal of a 1s electron from the Kr-like Au^{+43} ion. The ionization potential of Kr-like Au^{+43} is 2325 eV [18] and this ionization stage can be produced by electron temperatures of approximately 1/3 the ionization potential or 800 eV. The absence of these ions in Titan plasmas indicates the temperature is below 800 eV, or the electron temperature is higher and there is not sufficient time to produce high ionization in the transient plasma. In any case, it is clear that the Titan plasma conditions result in hard X-ray emissions that are dominated by electrons with energies exceeding 80 keV (based on the 1s binding energies listed in Table 2), and thermal processes play a minor role.

Evidently the abundant electrons with energies $>$ 80 keV, generated by fs laser pulse irradiation, efficiently produce 1s vacancies while lower energy thermal ($\leq$800 eV) electrons are insufficient to produce substantial ionization. In addition, the observation of brighter hard X-ray spectra from the thicker and larger targets irradiated by Titan laser pulses is consistent with the circulation of energetic electrons outside the focal spot. These observations are relevant to the transport of energy by fast electrons into dense material as necessary for the success of the fast ignition concept [19].

We note that such conclusions cannot be directly inferred from X-ray spectra with significantly lower energies because they can be affected by the large opacity of the dense Titan plasmas. Only high energy K-shell spectra from heavy metal targets are characteristic of the near solid density plasma produced by an intense fs laser pulse.

As seen in Table 3, the 1s–3p and 1s–4p transitions have the largest energy shifts from the neutral-atom transitions and are most useful for determining the ionization and temperature. When more well-exposed Au Kα and Kβ spectra become available, produced by higher energy fs laser irradiation, it should be possible to use the Au^{+26} 1s–3p and 1s–4p transitions, observed in the 2nd diffraction order of the DCS channel 2 crystal with higher resolution, to better determine the electron temperature.

The DCS channel 2 crystal with coverage to 120 keV is capable of recording K-shell spectra from U in the 95 keV to 115 keV energy range as listed in Table 2. However, the K-shell spectra produced by the present Titan laser diminish in brightness with atomic number, and more energetic and intense laser pulses will be necessary to record the K-shell spectra of the elements heavier than Au. Owing to the rapid advance in fs lasers, such observations are anticipated in the near future.

The spectral resolution of the DCS instrument can be increased by use of a crystal with smaller lattice spacing and higher dispersion, by use of a larger radius of curvature, and though ultimately limited by Rowland circle defocusing, by increasing the crystal-to-detector distance. Without altering the DCS geometry, laboratory studies were carried out with the NIST W anode X-ray source using a Ge (220) crystal with $2d = 4.00$ Å and bent to the same radius (254 mm) as the quartz (10–11) $2d = 6.686$ Å crystal. It was found that the Ge (220) crystal resulted in an energy scale accuracy of 40 eV, spectral line widths of 500 eV, and good resolution of the W $K\alpha_1$, $K\alpha_2$, $K\beta_1$, and $K\beta_2$ lines in the 1st diffraction order. However, direct comparison of the spectra recorded on image plates using the same X-ray dose indicated the 1st order spectrum produced by the Ge (220) crystal is a factor of two less intense than the 1st order spectrum produced by the quartz (10–11) crystal. Moreover, Au spectra were not observed on Titan shots when using a Ge (220) crystal in the DCS spectrometer. Thus when optimizing a spectrometer for the observation of the K-shell spectra of heavy metal targets, the quartz (10–11) crystal in the 2nd diffraction order has superior sensitivity and line width (400 eV) compared to the Ge (220) crystal in 1st order and bent to the same radius (500 eV line width).

Calculations of the diffraction efficiency of a flat quartz (10–11) crystal indicate efficiencies in the 1st, 2nd, and 3rd orders of 3.46, 1.93, and 0.42 microradians, respectively, at 70 keV energy. While the diffraction efficiencies of curved crystals can differ considerably from flat crystals, the calculated efficiencies suggest that it may be possible to utilize a quartz (10–11) crystal in the 3rd or higher orders to record high resolution hard X-ray spectra.

The absolute calibration of the DCS sensitivity can be carried out using an NIST calibrated laboratory W anode X-ray source and the NIST standard X-ray beam qualities. This would enable the implementation of quantitative diagnostic

techniques, based on hard X-ray K-shell spectroscopy, for understanding the laser energy deposition, energetic electron generation, ionization distribution, and X-ray conversion efficiency in plasmas produced by an intense fs laser pulse.

Acknowledgements

We thank the Titan laser operations staff for expert assistance. The work at NRL was supported by the Office of Naval Research. The work at LLNL was supported by the U.S. Department of Energy. The mention of a commercial produce does not represent an endorsement.

References

[1] L.T. Hudson, A. Henins, R.D. Deslattes, J.F. Seely, G.E. Holland, R. Atkin, L. Martin, D.D. Meyerhofer, C. Stoeckl, Rev. Sci. Instrum. 73 (2002) 2270.
[2] J.F. Seely, R. Doron, A. Bar-Shalom, L.T. Hudson, C. Stoeckl, J. Quant. Spectrosc. Radiat. Transf. 81 (2003) 421.
[3] J.F. Seely, C.A. Back, C. Constantin, R.W. Lee, H.-K. Chung, L.T. Hudson, C.I. Szabo, A. Henins, G.E. Holland, R. Atkin, L. Martin, J. Quant. Spectrosc. Radiat. Transf. 99 (2006) 572.
[4] L.T. Hudson, R. Atkin, C.A. Back, A. Henins, G.E. Holland, J.F. Seely, C. Szabo, Rad. Phys. Chem. 75 (2006) 1784.
[5] C.I. Szabo, L.T. Hudson, A. Henins, G.E. Holland, R. Atkin, J.F. Seely, Rad. Phys. Chem. 75 (2006) 1824.
[6] R.D. Deslattes, J.C. Levin, M.D. Walker, A. Henins, Med. Phys. 21 (1994) 123.
[7] C.T. Chantler, R.D. Deslattes, A. Henins, L.T. Hudson, Br. J. Radiol. 69 (1996) 636.
[8] L.T. Hudson, R.D. Deslattes, A. Henins, C.T. Chantler, E.G. Kessler, J.E. Schweppe, Med. Phys. 23 (1996) 1659.
[9] Hye-Sook Park, et al., Phys. Plasmas 13 (2006) 056309.
[10] W.C. Priedhorsky, D.W. Lier, R.H. Day, Rev. Sci. Instr. 54 (1983) 1605.
[11] G. Hölzer, E. Förster, M. Grätz, C. Tillman, S. Svanberg, J. X-Ray Sci. Technol. 7 (1997) 50.
[12] E. Andersson, G. Hölzer, E. Förster, M. Grätz, L. Kiernan, A. Sjögren, S. Svanberg, J. Appl. Phys. 90 (2001) 3048.
[13] R. Toth, J.C. Kieffer, A. Krol, S. Fourmaux, T. Ozaki, H. Ye, R.E. Kincaid, A. Rakhman, SPIE, vol. 5918 (2005) p. 1.
[14] R.D. Deslattes, E.G. Kessler, P. Indelicato, L. de Billy, E. Lindroth, J. Anton, Rev. Mod. Phys. 75 (2003) 35.
[15] Y. Amemiya, J. Synchrotron Rad. 2 (1995) 13.
[16] Hye-Sook Park, et al., Bull. Am. Phys. Soc. 51 (2006) 187.
[17] A. Bar-Shalom, M. Klapisch, J. Oreg, J. Quant. Spectrosc. Radiat. Transf. 71 (2001) 169.
[18] T.A. Carlson, C.W. Nestor, N. Wasserman, J.D. McDowell, At. Data 2 (1970) 63.
[19] R.R. Freeman, D. Batani, S. Baton, M. Key, R. Stephens, Fusion Sci. Technol. 49 (2006) 297.